Shape and Size Control of Artificial Cells for Bottom-Up Biology

Federico Fanalista*[1], Anthony Birnie*[1], Renu Maan[1], Federica Burla[2], Kevin Charles[1], Grzegorz Pawlik[1], Siddharth Deshpande[1], Gijsje H. Koenderink[2], Marileen Dogterom[1], Cees Dekker[$1]

[1] Department of Bionanoscience, Kavli Institute of Nanoscience Delft, Delft University of Technology, Van der Maasweg 9, 2629 HZ Delft, the Netherlands

[2] Department of Living Matter, Biological Soft Matter Group, AMOLF, Science Park 104, 1098 XG Amsterdam, the Netherlands

* Equal contribution

[$] Corresponding author: c.dekker@tudelft.nl

Supporting Information

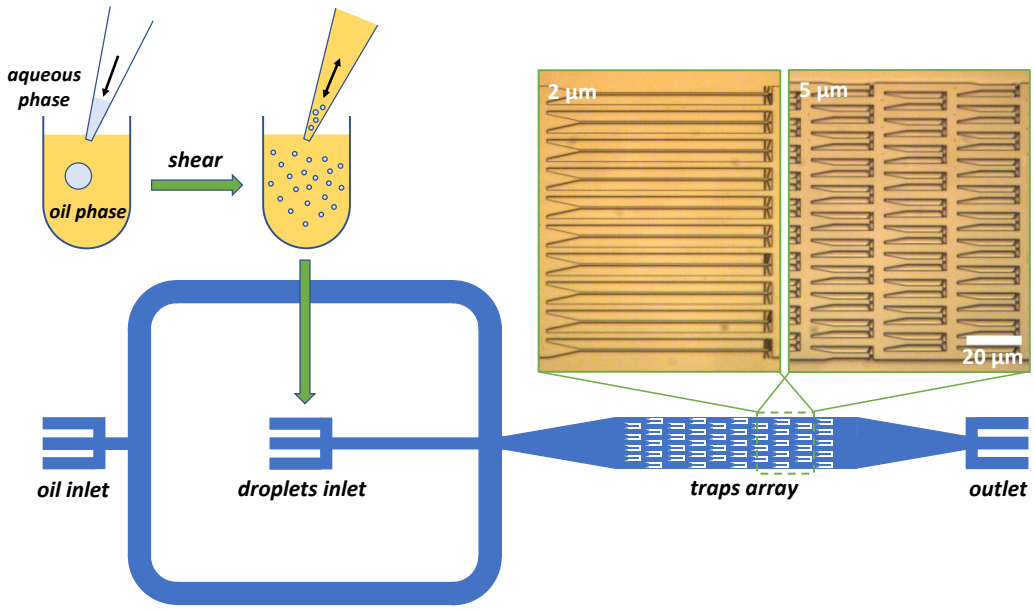

Figure S1. Schematic of the experimental procedure and device operation to obtain rod-shape droplets. A few microliters (2-5 µL) of an aqueous solution are pipetted into 100 µL of oil solution. Shear forces induced by repeatedly pipetting the solution up and down break the large droplets into smaller ones.[1] Droplet coalescence is prevented by surfactant molecules dissolved in the oil, which stabilize the water-oil interface of the droplets. The oil solution containing the droplets and a second oil solution without droplets are inserted via a pressure-driven pump into the device through two different inlets, as indicated. Past a junction where these two fluid streams meet, the droplets enter into a chamber containing an array of microfluidic traps. Once a satisfying number of droplets is caught at the entrance of the traps, the pressure of the outer oil stream is increased. In this way, the droplets get pushed inside the traps and thus deformed into the desired shape. The droplets that do not get caught by a trap are pushed towards the outlet and removed from the chamber. The pressure required to insert the droplets into the device is lower than the one required to insert the droplets inside the traps, and both pressures strongly depend on the dimensions of the device. As representative examples, two trap designs with dimensions on the

opposite sides of the size range explored in this work are visible in the bright-field microscopy images in the top right part of the figure. In the case of traps with a 5 µm x 5µm square cross-section (right), we experience that a minimum overpressure of ~0.1 bar is required to insert droplets into the device, which has to be increased to roughly ~0.2 bar to squeeze the droplets into the traps. For traps with a 2 µm x 2µm cross-section, the minimal overpressures required to insert droplets into the device and then into the traps are respectively around ~0.5 bar and ~0.8 bar. The droplets remained stably trapped as long as the pressure is kept constant. Otherwise, it is possible to release the droplets by lowering the pressure, as they slide back towards the entrance of the trap to minimize deformation. Alternatively, by increasing the pressure up to >1 bar, the droplets would eventually escape through the small exit holes of the traps. The detailed design of the traps varies depending on the final desired shape to be imposed on the artificial containers. Given that smaller structures require higher pressures, the walls of narrower traps are wider, in order to ensure that the trap walls remain bonded to the top PDMS membrane during the experiments. At the end of each trap, exit holes provide fluid flow through the structure. Generally speaking, the width of the exit hole equals half of the trap width. Also, to further facilitate the flow through the smaller traps, the number of lateral exit holes is increased. Finally, as the artificial containers preserve their original volume during deformation, the traps with smaller cross-sections are designed with an increased length. As the fluidic chamber containing the traps has the same dimension for all designs, the chamber contains a different number of traps depending on the trap dimensions: 57 for the 2 µm design and 105 for the 5 µm design. In principle the chamber can be designed as large as preferred, for example to accommodate a higher number of traps, as these devices are scalable, due the lithography-based method of fabrication.

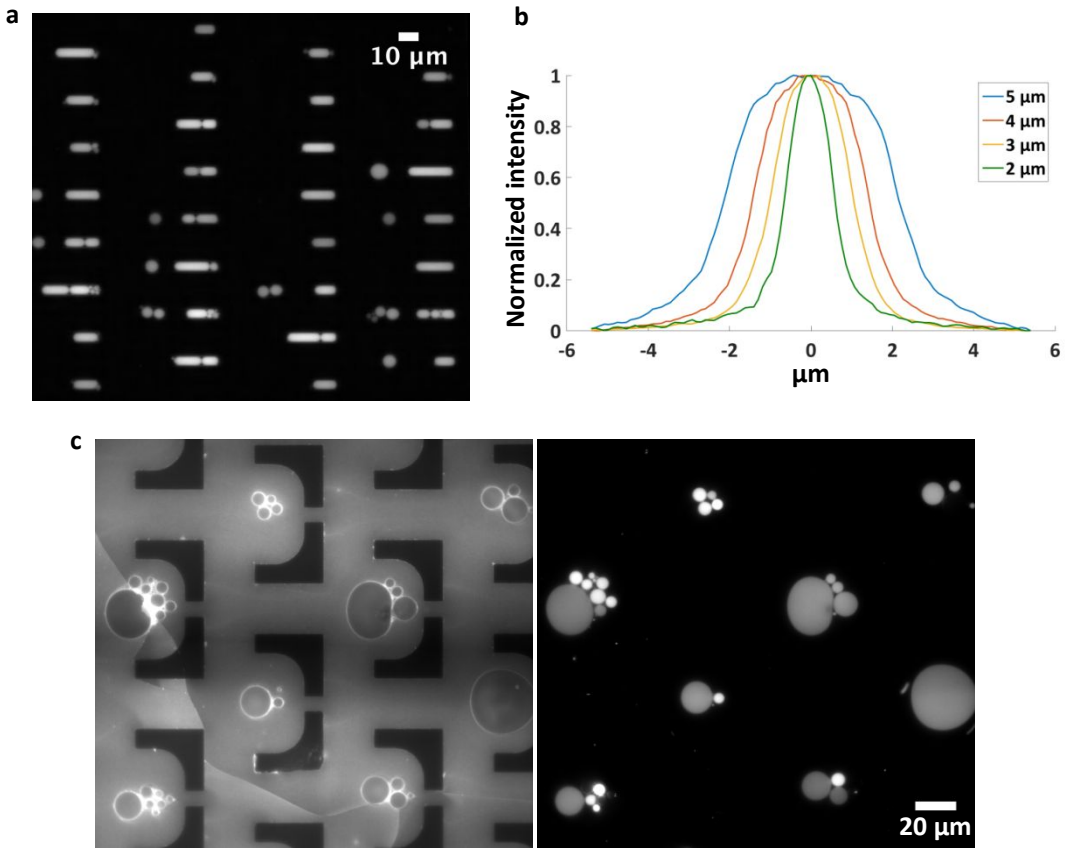

Figure S2. a) Array of 5 µm-wide microfluidic traps containing water-in-oil droplets. Fluorescent signal comes from Alexa 647 fluorescent dye in the aqueous phase. b) Normalized fluorescent profile of droplets in Figure 2b, measured at the mid-length equatorial cross section of tubular droplets over traps of different width. The plot shows the clear difference between the droplet widths. c) 2 µm high disc-shaped droplets immobilized in an array of microfluidic traps. On the left image, the fluorescence signal comes from fluorescent lipids dissolved in the oil phase and partitioned at the droplet interface, while on the right image fluorescent signal comes from Alexa 647 fluorescent dye in the aqueous phase.

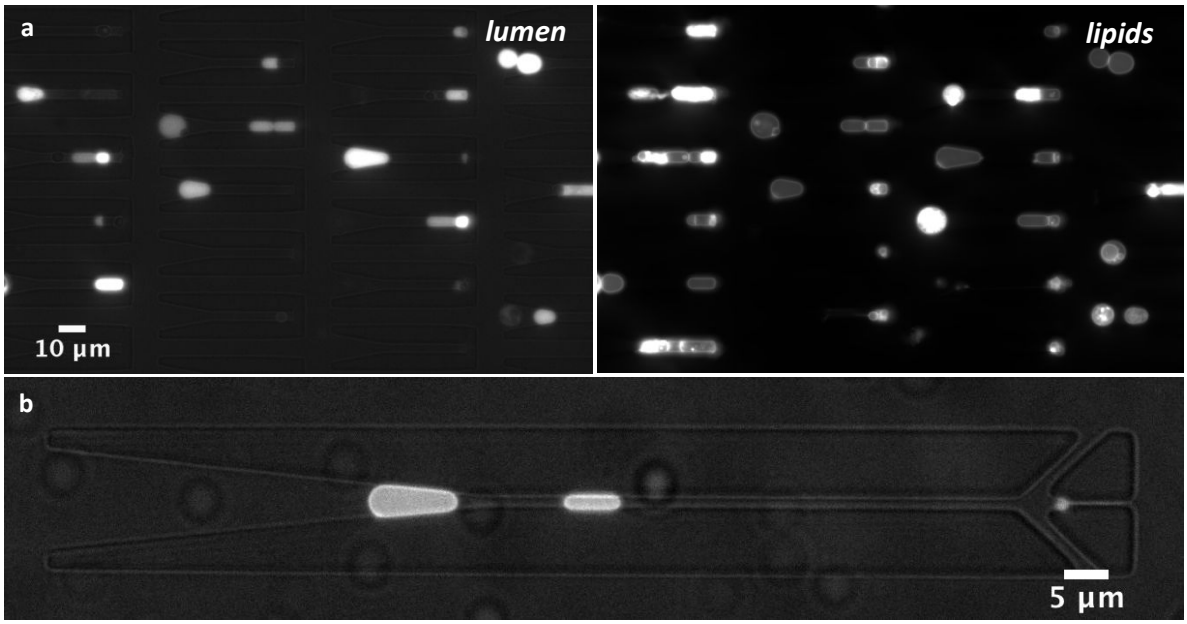

Figure S3. a) Array of tubular traps containing liposomes. Left: fluorescent signal coming from Alexa 647 inside the liposomes. Right: fluorescent signal coming from inclusion of Rhod PE embedded within the lipid membrane. Once trapped the resulting population shows some tense liposomes that did not enter into the traps, as well as liposomes that lost the fluorescent dye that was originally encapsulated at the moment of the production. We conjecture that the membrane floppiness induced by the osmotic pressure difference make the liposomes prone to split or simply to suffer temporary membrane defects during the insertion into the microfluidic chip, which would explain both the lack of membrane floppiness and loss of fluorescent dye from the lumen. b) Liposome deformed into a bacteria shape and size like *E. coli* (width ~1 μm).

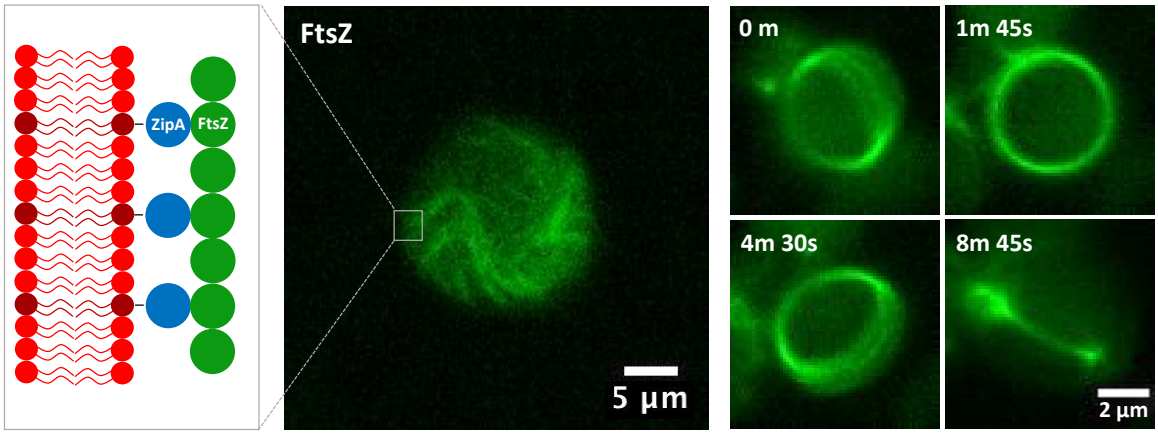

Figure S4. Reconstitution of FtsZ bundles inside unilamellar liposomes. As schematically illustrated on the left panel, FtsZ filaments bind to the lipid membrane by interacting with a soluble version of the membrane anchor protein ZipA. The arrangement of bundles on the liposome surface depends on the liposome size. In a population of liposomes (N = 10) with average diameter d = 9.2 ± 0.3 µm (middle) multiple randomly arranged bundles (n = 3.9 ± 0.2) are visible on the membrane. In contrast, a population of liposomes (N = 10) with a smaller diameter (d = 3.8 ± 0.2 µm), closer to the natural cell size, shows FtsZ bundles that are arranged in one single ring, as observed in the time lapse on the right. Fluorescent FtsZ signal comes from Alexa488 fluorescent dye.

Figure	Etch depth as measured by profilometer (μm)
2b, i (top); 3b; 6b; S1a	5.2
2b, ii	3.8
2b, iii	3.0
2b, iv (bottom); S2b	2.5
5c ii (bottom)	1.9
6a; 6c; 5b; 5c, i (top); S2a	5.3

Table S5. The etch depths of the wafers containing tubular traps used in the various figures. The measurements were done at three different points on the wafer using a profilometer. The quoted value is the mean of these measurements.

Category	Type	Largest dimension (µm)	Smallest dimension (µm)	Reference
Previous work	Spheres	3	3	12
		5	5	
		10	10	
		15	15	
		30	30	
		40	40	
		50	50	
	Discs	50	10	2
	Rods	11	5	3
		15	10	
		60	20	2
		300	110	4
This work	Discs	2	1	measured
		3	1	
		6	1	
		10	1	
		15	1	
		30	1	
	Rods	3	1.4	
		4	1.4	
		5	1.4	
		10	1.4	
		15	1.3	
		30	1.3	
		40	1.3	
		50	1.3	
Nature	*Escherichia coli*	2.05	0.63	5
		2.35	0.67	

		2.34	0.73	
		2.94	0.87	
	Saccharomyces cerevisiae	3	3	6
		6	6	
	Schizosaccharomyces pombe	7	3	3
		14	3	
	Bacillus subtilis	5	1	7
		10	2	
	S. aureus	0.9	0.82	8
	HeLa cells (grown as monolayers on polystyrene microcarrier beads)	20	10	9
	Red blood cell	8	2	10
	Cardiomyocyte	100	10	11
		100	25	
	Haloquadratum walsbyi	1.5	0.1	12
		11	0.5	
	Onion epidermis	300	80	13
	Filamentous *E. coli*	60	0.8	14
	Epulopiscium	600	80	15
	Mycoplasma (average size)	0.3	0.3	16

Table S6 Dimensions of deformable artificial cell containers and natural cells displayed in Figure 7. The dimensions of the artificial cell containers are taken from 'Previous Work' (spheres, discs and rods) and 'This Work' (discs and rods), whereas the 'Nature' section includes a representative selection of sizes and aspect ratios covered by natural cells used to sketch the blue area in Figure 7. For 'Previous Work', we selected spherical containers employed so far in the synthetic cell field. In addition, we included examples of previous attempts at deforming spherical containers into discs and rods. For 'This Work', we selected

the largest aspect ratios that we experimentally achieved for this paper. These points then form the lower boundary of the green area in Figure 7.

References

(1) Zieske, K.; Chwastek, G.; Schwille, P. Protein Patterns and Oscillations on Lipid Monolayers and in Microdroplets. *Angew. Chemie - Int. Ed.* **2016**, *55*, 13455–13459.

(2) Mellouli, S.; Monterroso, B.; Vutukuri, H. R.; Brinke, E. Te; Chokkalingam, V.; Rivas, G.; Huck, W. T. S. Self-Organization of the Bacterial Cell-Division Protein FtsZ in Confined Environments. *Soft Matter* **2013**, *9*, 10493–10500.

(3) Taberner, N.; Lof, A.; Roth, S.; Lamers, D.; Zeijlemaker, H.; Dogterom, M. *In Vitro* Systems for the Study of Microtubule-Based Cell Polarity in Fission Yeast. In *Methods in Cell Biology*; 2015; Vol. 128, pp 1–22.

(4) Boukellal, H.; Selimović, Š.; Jia, Y.; Cristobal, G.; Fraden, S.; Selimović, E.; Jia, Y.; Cristobal, G.; Fraden, S. Simple, Robust Storage of Drops and Fluids in a Microfluidic Device. *Lab Chip* **2009**, *9*, 331–338.

(5) Pierucci, O. Dimensions of Escherichia Coli at Various Growth Rates: Model for Envelope Growth. *J. Bacteriol.* **1978**, *135*, 559–574.

(6) Ahmad, M. R.; Nakajima, M.; Kojima, S.; Homma, M.; Fukuda, T. The Effects of Cell Sizes, Environmental Conditions, and Growth Phases on the Strength of Individual W303 Yeast Cells inside ESEM. *IEEE Trans. Nanobioscience* **2008**, *7*, 185–193.

(7) Marshall, W. F.; Young, K. D.; Swaffer, M.; Wood, E.; Nurse, P.; Kimura, A.; Frankel, J.; Wallingford, J.; Walbot, V.; Qu, X.; Roeder, A.H.K. What Determines Cell Size? *BMC Biol.* **2012**, *10*, 101.

(8) Maass, S.; Sievers, S.; Zühlke, D.; Kuzinski, J.; Sappa, P. K.; Muntel, J.; Hessling, B.; Bernhardt, J.; Sietmann, R.; Völker, U.; Hecker, M.; Becher, D. Efficient, Global-Scale Quantification of Absolute Protein Amounts by Integration of Targeted Mass Spectrometry and Two-Dimensional Gel-Based Proteomics. *Anal. Chem.* **2011**, *83*, 2677–2684.

(9) Zhao, L.; Kroenke, C. D.; Song, J.; Piwnica-Worms, D.; Ackerman, J. J. H.; Neil, J. J. Intracellular Water-Specific MR of Microbead-Adherent Cells: The HeLa Cell Intracellular Water Exchange Lifetime. *NMR Biomed.* **2008**, *21*, 159–164.

(10) Diez-Silva, M.; Dao, M.; Han, J.; Lim, C.-T.; Suresh, S. Shape and Biomechanical Characteristics of Human Red Blood Cells in Health and Disease. *MRS Bull.* **2010**, *35*, 382–388.

(11) Göktepe, S.; Abilez, O. J.; Parker, K. K.; Kuhl, E. A Multiscale Model for Eccentric and Concentric Cardiac Growth through Sarcomerogenesis. *J. Theor. Biol.* **2010**, *265*, 433–442.

(12) Albers, S.; Eichler, J.; Aebi, M. Chapter 22: Archaea. In *Essentials of Glycobiology*; Cold Spring Harbor Laboratory Press, 2015.

(13) Suslov, D.; Verbelen, J. P.; Vissenberg, K. Onion Epidermis as a New Model to Study the Control of Growth Anisotropy in Higher Plants. *J. Exp. Bot.* **2009**, *60*, 4175–4187.

(14) Lederer, F. L.; Günther, T. J.; Weinert, U.; Raff, J.; Pollmann, K. Development of Functionalised Polyelectrolyte Capsules Using Filamentous Escherichia Coli Cells. *Microb. Cell Fact.* **2012**, *11*, 163.

(15) Young, K. D. The Selective Value of Bacterial Shape. *Microbiol. Mol. Biol. Rev.* **2006**, *70*, 660–703.

(16) Zhao, H.; Dreses-Werringloer, U.; Davies, P.; Marambaud, P. Amyloid-Beta Peptide Degradation in Cell Cultures by Mycoplasma Contaminants. *BMC Res. Notes* **2008**, *1*, 38.